HHS Public Access

Author manuscript

Sci Transl Med. Author manuscript; available in PMC 2021 February 05.

Published in final edited form as:

Sci Transl Med. 2019 June 26; 11(498): . doi:10.1126/scitranslmed.aaw4636.

Arginine vasopressin receptor 1a is a therapeutic target for castration-resistant prostate cancer

Ning Zhao[1,2], **Stephanie O. Peacock**[2], **Chen Hao Lo**[3], **Laine M. Heidman**[1], **Meghan A. Rice**[2], **Cale D. Fahrenholtz**[1,*], **Ann M. Greene**[1], **Fiorella Magani**[2], **Valeria A. Copello**[2], **Maria Julia Martinez**[1,2], **Yushan Zhang**[4], **Yehia Daaka**[4], **Conor C. Lynch**[3], **Kerry L. Burnstein**[1,2,†]

[1]Department of Molecular and Cellular Pharmacology, Miller School of Medicine, University of Miami, Miami, FL 33136, USA.

[2]Sylvester Comprehensive Cancer Center, Miller School of Medicine, University of Miami, Miami, FL 33136, USA.

[3]Department of Tumor Biology, Moffitt Cancer Center, Tampa, FL 33612, USA.

[4]Department of Anatomy and Cell Biology, College of Medicine, University of Florida, Gainesville, FL 32610, USA.

Abstract

Castration-resistant prostate cancer (CRPC) recurs after androgen deprivation therapy (ADT) and is incurable. Reactivation of androgen receptor (AR) signaling in the low androgen environment of ADT drives CRPC. This AR activity occurs through a variety of mechanisms, including up-regulation of AR coactivators such as VAV3 and expression of constitutively active AR variants such as the clinically relevant AR-V7. AR-V7 lacks a ligand-binding domain and is linked to poor prognosis. We previously showed that VAV3 enhances AR-V7 activity to drive CRPC progression. Gene expression profiling after depletion of either VAV3 or AR-V7 in CRPC cells revealed arginine vasopressin receptor 1a (*AVPR1A*) as the most commonly down-regulated gene, indicating that this G protein–coupled receptor may be critical for CRPC. Analysis of publicly available human PC datasets showed that *AVPR1A* has a higher copy number and increased amounts of mRNA in advanced PC. Depletion of AVPR1A in CRPC cells resulted in decreased cell proliferation and reduced cyclin A. In contrast, androgen-dependent PC, AR-negative PC, or

†Corresponding author. kburnstein@med.miami.edu.

Author contributions: K.L.B., N.Z., S.O.P., Y.D., and C.C.L. designed the research. N.Z., S.O.P., C.H.L., L.M.H., M.A.R., C.D.F., A.M.G., V.A.C., and Y.Z. performed the research. F.M., V.A.C., and M.J.M. performed the computational analysis of online accessible data. N.Z., S.O.P., C.H.L., L.M.H., M.A.R., A.M.G., Y.Z., F.M., and K.L.B. analyzed the data. All authors interpreted the data. K.L.B and N.Z. wrote the paper.

*Present address: Department of Basic Pharmaceutical Sciences, Fred Wilson School of Pharmacy, High Point University, High Point, NC 27268, USA.

Competing interests: K.L.B. is an inventor on patent US 20160022635A1 submitted by University of Miami that covers “Use of arginine vasopressin receptor antagonists for the treatment of prostate cancer”. All other authors declare that they have no competing interests.

Data and materials availability: The microarray data that support the findings of this study have been deposited in the GEO repository with the accession code GSE104572. All data associated with this study are present in the paper or in the Supplementary Materials.

SUPPLEMENTARY MATERIALS

stm.sciencemag.org/cgi/content/full/11/498/eaaw4636/DC1

nontumorigenic prostate epithelial cells, which have undetectable *AVPR1A* mRNA, were minimally affected by AVPR1A depletion. Ectopic expression of AVPR1A in androgen-dependent PC cells conferred castration resistance in vitro and in vivo. Furthermore, treatment of CRPC cells with the AVPR1A ligand, arginine vasopressin (AVP), activated ERK and CREB, known promoters of PC progression. A clinically safe and selective AVPR1A antagonist, relcovaptan, prevented CRPC emergence and decreased CRPC orthotopic and bone metastatic growth in mouse models. Based on these preclinical findings, repurposing AVPR1A antagonists is a promising therapeutic approach for CRPC.

INTRODUCTION

Androgen-deprivation therapy is the standard treatment for advanced prostate cancer (PC). Despite initial responses, including symptomatic relief and decreased circulating prostate-specific antigen (PSA), PC recurs in 1 to 3 years and typically is accompanied by rising PSA. The recurrent PC is termed castration-resistant PC (CRPC), an incurable and more rapidly progressing disease state. CRPC arises and progresses due to reactivation of androgen receptor (AR) signaling, occurring through multiple nonmutually exclusive mechanisms resulting in a distinct reprogrammed transcriptome (1, 2).

VAV3, a Rho family guanosine triphosphatase guanine nucleotide exchange factor, is a versatile coactivator of AR in PC and confers castration resistance to androgen-dependent PC in vivo (3-5). Increased VAV3 correlates with poor clinical outcome for PC (6). VAV3 enhances the activity of multiple, clinically relevant forms of AR in PC, including constitutively active variants such as AR-V7 (7), which is thought to be an important driver of castration resistance (8, 9). We sought to identify common downstream gene targets of VAV3 and AR-V7 because of their critical roles in CRPC. Through inducible depletion of VAV3 or AR-V7 and gene expression profiling of CRPC cells, we identified arginine vasopressin receptor 1a (*AVPR1A*) as the most down-regulated dual target gene of AR-V7 and VAV3. AVPR1A is a member of the heteromeric G protein (heterotrimeric guanine nucleotide–binding protein–coupled receptor (GPCR) family that signals via G proteins Gq/11 in classical target tissues (10). The three vasopressin receptor subtypes, AVPR1A, AVPR1B, and AVPR2, have the same physiological ligand, arginine vasopressin (AVP), but are distinct in their tissue expression profiles and functions. AVPR1A is expressed in the vascular smooth muscle cells, cardiomyocytes, hippocampus, kidney, bone, liver, and select breast and non–small cell lung cancer cell lines (11-18). An orally available selective AVPR1A antagonist, relcovaptan, has shown efficacy and safety in clinical trials of Raynaud's syndrome, dysmenorrhea, and preterm labor (19, 20). Relcovaptan was well tolerated, and no side effects were reported in clinical trials (21, 22).

Publicly available datasets from human PC specimens show that a substantial proportion of men with CRPC present with *AVPR1A* gene copy number amplification, and there are also increased amounts of *AVPR1A* mRNA in advanced PC cases compared to primary disease (23-25). We demonstrate that AVPR1A depletion greatly decreased CRPC growth but had negligible effect in androgen-dependent PC, AR-negative PC, or nontumorigenic prostate epithelial cells, which did not express detectable *AVPR1A* mRNA. AVPR1A conferred

castration resistance to androgen-dependent PC in vitro and in vivo. Relcovaptan substantially inhibited tumor growth in three distinct highly relevant preclinical PC settings: an early CRPC progression model, a local CRPC invasion model, and an end-stage CRPC model of growth in the bone metastatic niche. Together, our findings indicate that AVPR1A is a promising therapeutic target for CRPC that can be translated rapidly to the clinic because of the existence of safe and effective antagonists established in phase 1 and 2 clinical trials.

RESULTS

AVPR1A is dually regulated by AR-V7 and its coactivator, VAV3, in CRPC cells

To identify downstream genes that were regulated by VAV3 and AR-V7, we conducted gene expression profiling by inducibly depleting VAV3, AR-V7, or green fluorescent protein (GFP) (control) in the CRPC cell line, 22Rv1. We identified a group of genes commonly down-regulated by either shVAV3 or shAR-V7 but not the shGFP control (Fig. 1A). *AVPR1A* was the most down-regulated gene after either VAV3 or AR-V7 depletion (table S1) and is potentially druggable given the available antagonists to this GPCR (19). The regulation of *AVPR1A* mRNA by VAV3 and AR-V7 was confirmed by stable depletion of VAV3 or AR-V7 in 22Rv1 cells (Fig. 1B). To validate this finding in vivo, we examined *AVPR1A* mRNA in human PC vertebral-cancer of the prostate (VCaP) xenograft tumors [in severe combined immunodeficient (SCID) mice] obtained from our previous study (5). These VCaP xenografts (overexpressing VAV3 or GFP control vector) were obtained before and after progression to castration resistance in vivo through orchiectomy (5). Androgen-dependent VCaP tumor growth plateaus after castration but eventually resumes, indicative of the castration resistance phenotype (26, 27). Progression to castration resistance in this VCaP xenograft model is accompanied by AR-V7 up-regulation (28) and similarly, AR-V7 was increased in these VCaP castration-resistant tumors compared to androgen-dependent tumors (7). We found that *AVPR1A* mRNA was increased in CRPC xenograft tumors overexpressing VAV3 compared to tumors generated from VCaP cells expressing control vector (Fig. 1C). Hence, *AVPR1A* was up-regulated under conditions of enhanced AR-V7 and VAV3 signaling in CRPC cells.

AVPR1A mRNA is expressed in greater amounts in advanced human PC specimens compared to primary disease

To determine whether there are alterations in the *AVPR1A* gene and mRNA in PC specimens compared to noncancer, we first queried cBioPortal to analyze The Cancer Genome Atlas (TCGA) PC provisional dataset, containing RNA expression profiles of primary tumors (29-31). Only 5% of the primary prostate tumor samples contain *AVPR1A* gene alterations (missense mutation, amplification, or deep deletion) or increased amounts of *AVPR1A* mRNA (fig. S1A). Similarly, only 7% of these samples exhibit increased *AR* gene copy number or have up-regulated *AR* mRNA (fig. S1A). In contrast, human PC expression profile datasets revealed that *AVPR1A* mRNA in CRPC is substantially increased compared to hormone-sensitive androgen-dependent PC (Fig. 1D). *AVPR1A* mRNA in human metastatic PC is also increased compared to primary site (prostate) cancer (Fig. 1E) (24, 25). In the Beltran *et al.* (23) CRPC dataset, 21% of human CRPC specimens exhibited

higher *AVPR1A* gene copy number compared to their germline counterparts (Fig. 1F) [cBioPortal analysis (23, 29, 30)]. Within this dataset, there was a similar frequency of patients with *AVPR1A* gene amplification in adenocarcinoma CRPC (11 of 51 patients) and neuroendocrine CRPC tumors (6 of 30 patients). In addition, amounts of *AVPR1A* and *VAV3* mRNA were higher in the metastases of patients with AR-V7–positive CTCs (circulating tumor cells; a marker of late stage disease, especially metastasis) compared to metastases from patients whose CTCs did not express AR-V7 (fig. S1B) (32, 33). Together, these data indicate that *AVPR1A* mRNA is increased in advanced and CRPC compared to primary PC.

AVPR1A depletion inhibits CRPC proliferation

Because greater amounts of *AVPR1A* mRNA are present in advanced and metastatic human PC samples, we examined the expression and possible actions of this receptor in PC cells. AR-positive CRPC cell lines (22Rv1, CWR-R1, C4-2B, and LNCaP-abl) expressed detectable *AVPR1A* mRNA, but in the AR-negative PC lines (PC3 and DU145), androgen-dependent LNCaP, or a nontumorigenic prostate epithelial cell line (RWPE-1), *AVPR1A* mRNA was not detected (fig. S2). LNCaP-abl and C4-2B are derived from androgen-dependent LNCaP cells, indicating that *AVPR1A* mRNA expression was correlated with castration resistance (fig. S2).

Depletion of *AVPR1A* mRNA in AVPR1A-expressing CRPC cells resulted in a large decrease in proliferation (Fig. 2A). Transduction of shAVPR1A in DU145, LNCaP (PC cell lines), and RWPE-1 (nontumorigenic prostate epithelial cells), which do not express detectable *AVPR1A* mRNA (fig. S2), had no effect on cell proliferation (fig. S3A). Although the amount of *AVPR1A* mRNA was below the detectable limit in PC3 (a PC cell line), there was a modest decrease in proliferation after transduction of shAVPR1A (fig. S3A). Thus, we cannot rule out the possibility that these cells express some AVPR1A.

We investigated possible mechanisms of inhibition of CRPC cell proliferation mediated by AVPR1A depletion. Cyclin A, a G_1-S cell cycle marker, was down-regulated in 22Rv1, CWR-R1, and LNCaP-abl cells after AVPR1A knockdown (Fig. 2B). Cleaved poly(adenosine diphosphate–ribose) polymerase (PARP), an apoptosis marker, was up-regulated in 22Rv1, CWR-R1, and C4-2B cells after AVPR1A knockdown (Fig. 2B). As expected, depletion of AVPR1A did not produce similar effects on these cell cycle or apoptosis markers in cells lacking detectable *AVPR1A* mRNA (fig. S3B). Thus, regulation of both cell cycle and apoptosis is implicated in the antiproliferative effects observed in CRPC cells depleted of AVPR1A.

To ensure that the antiproliferative effects that occurred with shAVPR1A transduction in CRPC cell lines were because of selective depletion of AVPR1A, we designed two additional short hairpin RNA (shRNA) constructs that targeted different regions of *AVPR1A* mRNA. All three shAVPR1A constructs decreased *AVPR1A* mRNA and inhibited 22Rv1 cell growth (fig. S4, A and B). The shAVPR1A-7 had both the greatest knockdown efficiency and the greatest inhibition of 22Rv1 cell proliferation (fig. S4, A and B) and was therefore used in Fig. 2 and fig. S3. We also performed rescue experiments using the 3′ untranslated region (3′UTR)–targeted shAVPR1A construct and a hemagglutinin (HA)–

tagged AVPR1A expression vector lacking the 3′UTR, making this vector resistant to shRNA-mediated depletion (fig. S4C). Forced expression of knockdown-resistant AVPR1A rescued the 22Rv1 cells from shAVPR1A-mediated growth inhibition (fig. S4D).

AVPR1A confers castration-resistant growth in vitro and in vivo

To determine whether AVPR1A conferred castration resistance, we used the androgen-dependent cell line LNCaP, which has impeded growth in androgen-depleted medium (34). We stably expressed AVPR1A in LNCaP, which lack detectable *AVPR1A* mRNA (fig. S2) and cultured cells in medium supplemented with charcoal-stripped serum (CSS), lacking steroids (including androgens), to mimic castration conditions. In contrast to control cells expressing empty vector, LNCaP/AVPR1A grew more rapidly in castration conditions (Fig. 3A). Because of the lack of high-quality, specific AVPR1A antibodies, we verified ectopic AVPR1A expression by its HA-tag (Fig. 3B). Thus, AVPR1A expression alone conferred castration resistance in androgen-dependent cells in vitro. To investigate whether AVPR1A conferred castration resistance in vivo, we used a mouse xenograft tumor model that progresses to castration resistance (Fig. 3C). Empty vector control or AVPR1A-overexpressing LNCaP cells were injected subcutaneously into the hind flanks of nude mice. Mice were castrated when tumors reached 100 to 150 mm^3. LNCaP/AVPR1A xenografted tumors grew faster than LNCaP control tumors, indicating that AVPR1A promoted castration resistance in vivo (Fig. 3C).

AVPR1A signals through mitogenic pathways that are blocked by pharmacologic inhibition in CRPC

The natural ligand of AVPR1A (and the other vasopressin receptor subtypes, AVPR1B and AVPR2) is AVP (also known as antidiuretic hormone) (15). Consistent with AVPR1A signaling via Gq/11 and phospholipase C, AVP stimulated calcium release from the endoplasmic reticulum in a dose-dependent manner in 22Rv1 cells (Fig. 4A). This AVP-induced calcium release in 22Rv1 cells was blocked by relcovaptan (SR49059), a highly selective AVPR1A antagonist (Fig. 4A) (35). Sensitivity to AVP-stimulated calcium release in PC cell lines correlated with presence of endogenous *AVPR1A* mRNA (figs. S2 and S5, A and B). Overexpression of AVPR1A in nontumorigenic prostate epithelial cells, RWPE-1, was sufficient to elicit a calcium response upon AVP stimulation (fig. S5B). Together, these results indicate that AVP-stimulated AVPR1A signaling in CRPC cells can be blocked by the subtype selective antagonist relcovaptan.

AVP mediates increased cell survival or growth via ERK phosphorylation in well-studied target cells (cardiac myoblasts and vascular smooth muscle cells) (36-39). We found that ERK phosphorylation was induced in 22Rv1 CRPC cells upon AVP stimulation in a dose- and time-dependent manner (Fig. 4B). AVP-stimulated ERK phosphorylation was blocked by relcovaptan, implying that AVP-induced ERK phosphorylation proceeds through AVPR1A and not through other AVPR subtypes (Fig. 4C).

To begin to define how AVPR1A regulated CRPC growth and survival, we used phosphoproteomic kinase arrays that interrogate 43 distinct signaling phosphorylation sites. AVP increased ERK phosphorylation as expected based on experiments shown in Fig. 4B

(fig. S6A). However, CREB was also phosphorylated in response to AVP (fig. S6A). Relcovaptan blocked AVP-induced phosphorylation of both proteins (fig. S6A). Subsequently, we found that an ERK inhibitor, PD98059, blocked AVP-stimulated CREB phosphorylation, indicating that AVP signals via the AVPR1A/ERK/CREB pathway in CRPC cells (Fig. 4D). Although AVP acutely activated mitogenic pathways in CRPC cells, long-term (up to 6 days) treatment of CRPC cells with AVP did not affect cell proliferation (fig. S6B).

AVPR1A antagonism decreases CRPC tumor growth in three distinct preclinical settings

To examine AVPR1A antagonism as a potential therapeutic approach for CRPC, we adopted a preclinical xenograft model that reproduces the progression of PC from androgen dependence to castration resistance (5). Androgen-dependent VCaP cells were injected subcutaneously into SCID mice, which were castrated when tumors reached about 250 mm^3. Once the androgen-dependent VCaP tumors acquired castration resistance (the time point at which tumor growth reinitiated after a plateau phase), relcovaptan was administered orally on a daily basis for 2 weeks. Treatment with relcovaptan halted tumor growth (Fig. 5A) and stabilized circulating PSA (a clinical marker of progression secreted solely by human PC cells and not by rodents) (Fig. 5B). Furthermore, immunohistochemical analysis of tumor tissues showed decreased Ki67 (a proliferative marker) staining in relcovaptan-treated mice compared to mice receiving vehicle (Fig. 5, C and D). Western blotting of the tumor lysates revealed that cyclin A was down-regulated by relcovaptan (Fig. 5E), similar to observations after AVPR1A depletion in CRPC cells in culture (Fig. 2B). These results indicate that inhibition of AVPR1A blocks or delays the emergence of CRPC.

We used an orthotopic xenograft model to examine the ability of relcovaptan to inhibit established CRPC tumor growth in mouse prostates, mimicking CRPC primary growth and local invasion. We used C4-2B, a highly aggressive CRPC cell line derived from LNCaP cells. Luciferase-labeled C4-2B cells were injected into the prostates of SCID mice, followed immediately by castration. The C4-2B tumors were established within 2 weeks (based on IVIS imaging), and mice were given either relcovaptan or vehicle orally daily for 6 weeks. Relcovaptan substantially mitigated aggressive CRPC growth in mouse prostates compared to vehicle-treated controls (Fig. 5F).

PC typically metastasizes to the skeleton, generating both bone-destructive and bone-forming lesions, which are regulated by osteoclasts and osteoblasts, respectively (40). To mimic the growth of late-stage CRPC in bone, luciferase-labeled C4-2B cells were introduced directly into the tibias of castrated SCID mice. Similar to the subcutaneous and orthotopic tumor models, relcovaptan decreased castration-resistant tumor growth in the bone microenvironment (Fig. 6, A and B). Over the 83 days of treatment, relcovaptan did not affect mouse body weights (Fig. 6C), appetite, or general behavior. Instead, relcovaptan substantially improved mouse survival rate by prolonging the time to reach the predetermined maximal tumor burden (Fig. 6D).

Genetic deletion or pharmacological inhibition of AVPR1A limits bone remodeling (41). We therefore assessed the impact of relcovaptan on CRPC-induced bone disease. C4-2B cells commonly generate osteogenic lesions in in vivo bone metastasis models (42). As expected,

high-resolution micro–computed tomography (μCT) demonstrated that vehicle-treated tumor-bearing tibias display much higher bone-to-total volume ratio (BV:TV) than vehicle-treated tumor-naïve tibias (sham) (Fig. 6E). Relcovaptan administration in tumor-bearing tibias presented BV:TV comparable to BV:TV of vehicle-treated tumor-naïve tibias, potentially indicating that relcovaptan disrupted the PC-to-bone signaling resulting in preserved normal bone status (Fig. 6E). Furthermore, relcovaptan treatment had negligible effects on BV:TV in tumor-naïve tibias (Fig. 6E). Analyses of BV:TV in tissue sections by immunohistochemistry confirmed μCT results (Fig. 6, F to I).

DISCUSSION

Our unbiased transcriptomic studies designed to define downstream targets of AR-V7 and the versatile AR coactivator, VAV3, in CRPC resulted in the identification of *AVPR1A* as a dually regulated target gene. We prioritized the evaluation of AVPR1A as a potential therapeutic target for PC because *AVPR1A* mRNA is increased in aggressive PC compared to primary disease and clinically safe and effective subtype-selective AVPR1A antagonists are available (19, 43). Both AVPR1A depletion and ectopic expression studies support the contention that AVPR1A is sufficient to drive CRPC progression. Preclinical experiments showed that AVPR1A blockade with relcovaptan inhibited CRPC in three distinct preclinical stages of human disease: newly emergent CRPC, primary and locally invasive established CRPC, and CRPC growth in the late-stage bone metastatic niche. This study describes AVPR1A as an actionable therapeutic target for CRPC, as summarized in the model (fig. S7).

AVPR1A mRNA is expressed in several human small cell lung and breast cancer cell lines, where it appears to have proproliferative effects (36-39, 44). Consistent with a mitogenic/prosurvival role of AVPR1A, we found that AVPR1A depletion resulted in substantial growth inhibition in CRPC cells. AVPR1A was expressed in the AR-positive CRPC cell lines: 22Rv1, CWR-R1, and the LNCaP CRPC derivatives LNCaP-abl and C4-2B. In contrast, *AVPR1A* mRNA was below the limits of detection in androgen-dependent LNCaP, AR-negative PC cell lines PC3 and DU145, and nontumorigenic prostate epithelial cells RWPE-1. The lack of reliable anti-AVPR1A antibodies precluded our ability to demonstrate either native or overexpressed AVPR1A protein in CRPC cells. Although we first identified *AVPR1A* as a dual target of VAV3 and AR-V7, the basis for the expression of AVPR1A in an AR-positive line such as C4-2B CRPC, which lacks AR-V7, is unknown and will need to be investigated in future studies.

The physiologic ligand, AVP, stimulated rapid canonical responses in AVPR1A-expressing PC cells, including intracellular calcium release and phosphorylation of ERK. These effects were blocked by the AVPR1A subtype-selective antagonist, relcovaptan, consistent with AVPR1A signaling via Gq/11 in CRPC. Furthermore, forced expression of AVPR1A in nontumorigenic prostate epithelial cells evoked AVP-mediated calcium release, indicating that receptor expression was sufficient and therefore that prostate lineage cells retain the other components of this signaling pathway.

Phosphoproteomic assays revealed that CREB was phosphorylated in response to AVP treatment, and its phosphorylation was through AVPR1A signaling based on inhibition by relcovaptan. CREB mediates PC progression (45-49) and has been reported to promote PC bone metastasis (50, 51). Further analysis suggests that AVP signals via an AVPR1A/ERK/CREB pathway in CRPC. CREB regulates the transcription of cell cycle genes, such as cyclin A and cyclin D1 (52-54). We observed that AVPR1A depletion or antagonism decreased cyclin A, consistent with ERK/CREB signaling in CRPC cell proliferation. Despite the finding that AVP acutely promoted proproliferative and survival signaling, AVP did not stimulate CRPC cell proliferation. The lack of such AVP-mediated long-term effects may be due to differences in culture conditions because cell proliferation experiments need to be conducted in serum-containing medium. Under these conditions, AVPR1a may be sufficiently active without additional ligand. We found that AVPR1A depletion greatly decreased CRPC cell proliferation and that ectopic expression of AVPR1A was sufficient for castration-resistant growth.

We used the commercially available relcovaptan for preclinical assessment of AVPR1A antagonism in PC. This small-molecule inhibitor can be given orally, exhibits subtype specificity (35, 55), and has been effectively and safely used in several clinical trials for Raynaud's syndrome, dysmenorrhea, and preterm labor (20, 22). In addition, other vaptan-type AVPR1A antagonists are currently under clinical investigation for anxiety, post-traumatic stress disorder, autism, and other behavioral indications; thus, AVPR1A antagonists' safety and efficacy for long-term use is being established (clinical trial identifier: NCT03504917, NCT03036397, and NCT02922166) (56).

Relcovaptan decreased CRPC growth in three preclinical mouse models: newly emergent castration-resistant disease, established CRPC in prostate (orthotopic) xenografts, and late-stage bone metastasis after intratibial injection of CRPC cells. Although relcovaptan greatly decreased tumor growth, xenografts did not appear to regress in any of the three in vivo models. Relcovaptan in combination with other standard PC therapeutic approaches may result in complete tumor regression, which should be investigated in future studies.

Relcovaptan also protected against cancer-induced bone disease. PC cells promote osteoclast and osteoblast activity with the resultant increase in bone remodeling, releasing growth factors such as transforming growth factor β that can promote PC cell survival and growth in the bone microenvironment. AVPR1A is an important regulator of osteoclast function (41), and limiting osteoclast function by relcovaptan may have clinical relevance by preventing the CRPC cells from access to bone-derived growth and survival factors. In the context of the tumor-bone microenvironment, we therefore posit that relcovaptan may directly and indirectly limit CRPC growth.

Our preclinical data indicate that pharmacological targeting of AVPR1A is efficient and effective. We did not observe any obvious toxicity of relcovaptan, and AVPR1A inhibition had benefit for end-stage bone-metastatic CRPC, for which therapeutic options are limited. Although relcovaptan inhibited CRPC growth in three mouse models with distinct tumor microenvironments, a limitation of our study is the use of human cell lines in immunocompromised mouse tumor xenograft models. Together, the data support

therapeutically targeting AVPR1A as a treatment strategy for aggressive PC, including for bone-metastatic CRPC, and for alleviating or preventing skeletal-related diseases and pain to improve patients' quality of life and survival.

MATERIALS AND METHODS

Study design

The aims of this study were to define the function of the GPCR AVPR1A in CRPC and to evaluate the feasibility of pharmacological targeting of AVPR1A in PC tumor-bearing mice. We confirmed one potential role of AVPR1A in CRPC cell growth through complementary loss-of-function and gain-of-function experiments. To assess whether AVPR1A is a potential treatment target, we evaluated its antagonist relcovaptan in cellular signaling and in CRPC xenograft studies in mice. All the original data are in data file S1.

All cell-based experiments (cell proliferation and calcium imaging) were conducted and confirmed with at least three independent experiments, which were each performed in triplicate or more. Gene knockdown was confirmed by RT-qPCR, and gene overexpression was confirmed by RT-qPCR and Western blotting.

In the subcutaneous xenograft mouse model, mouse numbers were calculated to achieve greater than 93% statistical power to detect a 30% decrease in tumor volume with 10% attrition. In orthotopic and intratibial injection mouse models, mouse numbers were calculated to achieve more than 93% statistical power to detect a mean difference of twofold change in photon flux between the two treatment groups on ex vivo imaging. The mice were randomized into trial groups by Research Randomizer (www.randomizer.org). Subcutaneous xenograft tumors were measured blindly. However, all IVIS imaging was performed in an unblinded fashion. Data collection and end points followed the planned timeframes, which allowed adequate time for tumor growth and avoided loss of mice due to excessive tumor burden.

Once the PC cells were inoculated into mice, mice were only removed from the studies when: (i) there was premature death due to unspecified cause and (ii) health issues, such as loss of 20% body weight. For the study shown in Fig. 3C, no mice from the xenograft vector group (LNCaP expressing vector) and one mouse from the AVPR1A group were removed. In Fig. 5A, two vehicle-treated mice and two relcovaptan-treated mice were removed. In Fig. 5F, five vehicle-treated mice and seven relcovaptan-treated mice were removed. In Fig. 6A, no vehicle-treated mice and one relcovaptan-treated mouse were removed. In Fig. 6A, some mice achieved excessive tumor burden before the predetermined study end point; they were humanely euthanized, and the data from these mice were included in the final results.

Once all the raw data were collected, the unqualified data were removed before analysis. The criteria for exclusion were: (i) for subcutaneous xenografting, the injection needle penetrated the muscle layer; (ii) for orthotopic xenografting, no tumor was established in the prostate; (iii) for intratibial xenografting, μCT scanning confirmed tumor growth outside of the tibial bone; or (iv) IVIS image collection failed.

Cell culture and reagents

Human PC cell lines CWR-22Rv1 (CRL-2505), LNCaP [the American Type Culture Collection (ATCC), catalog no. CRL 1740], and human prostate epithelial cell line RWPE (CRL-11609) were obtained from ATCC. CWR-R1, VCaP, LNCaP-abl, and C4-2B cells were gifts from fellow scientists (see Acknowledgments). Virus packaging cell lines Lenti-X and GP2-293 were obtained from Clontech. All cell lines were negative for mycoplasma, bacteria, and fungi contamination and were authenticated using short tandem repeat (Genetica) on 26 February 2016. 22Rv1, CWR-R1, and LNCaP cells were cultured in RPMI (Corning) supplemented with penicillin (100 IU/ml), streptomycin (100 μg/ml), 2 mM L-glutamine (Life Technologies Inc.), and 10% fetal bovine serum (FBS) (Atlanta Biologicals). LNCaP-abl were cultured in phenol-free RPMI (Gibco) supplemented with penicillin (100 IU/ml), streptomycin (100 μg/ml), 2 mM L-glutamine, and 10% CSS (Thermo Fisher Scientific). VCaP cells were cultured in Dulbecco's modified Eagle's medium (DMEM) GlutaMAX (Gibco) supplemented with penicillin (100 IU/ml), streptomycin (100 μg/ml), amphotericin B (250 ng/ml) (Gibco), and 10% FBS. C4-2B, Lenti-X, and GP2-293 cells were cultured in DMEM (Corning) supplemented with penicillin (100 IU/ml), streptomycin (100 μg/ml), 2 mM L-glutamine, and 10% FBS. RWPE-1 cells were cultured in keratinocyte serum-free medium supplemented with full growth factor kits (Gibco). For proliferation assays, 22Rv1, CWR-R1, PC3, and DU145 were cultured with 2% FBS. LNCaP-abl cells were cultured with 2% CSS, and C4-2B cells were cultured with 10% CSS. ShGFP and shAVPR1A-transduced cells were cultured with puromycin (500 ng/ml) (Sigma-Aldrich). Empty vector and AVPR1A-transduced cells were cultured with G418 (300 μg/ml) (Corning). All cell lines were used within five passages after authentication. Cell cultures were maintained at 37°C in a humidified atmosphere of 5% CO_2. AVP and PD98059 were purchased from Sigma-Aldrich. Relcovaptan (SR 49059) was purchased from Axon Medchem.

Microarray

Three independent 22Rv1 cell isolates were derived after transduction of shRNAs (tet-pLKO shGFP, tet-pLKO shAR-V7, and tet-pLKO shVAV3). Cells were grown in 10% CSS in the presence or absence of doxycycline for 24 to 72 hours. Knockdown was evaluated via Western blot from a parallel protein harvest. Seventy-two hours after the induction of knockdown, RNA from the 18 samples was sent to the University of Miami Genetics Core for RNA integrity number evaluation and microarray analysis. GC robust multi-array average (RMA) package was used for the analysis. Differences in mRNA amounts upon doxycycline treatment were examined ($P < 0.05$), and genes mutually regulated by shAR-V7 or shVAV3 were identified. Genes, whose expression was significantly different in the shGFP control upon doxycycline treatment ($P < 0.05$), were removed from the list of common targets of AR-V7 and VAV3.

Bioinformatic analysis of AVPR1A

The "TCGA" and "Beltran" datasets were accessed and analyzed through cBioPortal, as previously described (23, 29-31). The publicly available Tamura (accession no. GSE6811) and Chandran (accession no. GSE6752) datasets were retrieved from the NCBI GEO

database (www.ncbi.nlm.nih.gov/gds). The *AVPR1A* expression values in both datasets were presented as log2-transformed signal intensity ratios. Preprocessed *AVPR1A* RNA sequencing data of CTCs were obtained from GEO database (GSE56701), and reads per kilobase per million mapped reads values from AR-V7–positive ($n = 2$) and AR-V7–negative ($n = 2$) CTC patient samples were averaged.

In vitro cell proliferation assay

For the shAVPR1A knockdown assay, 22Rv1 (7500 cells per well), CWR-R1 (10,000 cells per well), LNCaP-abl (10,000 cells per well), C4-2B (10,000 cells per well), LNCaP (5000 cells per well), and RWPE-1 (5000 cells per well) were seeded in 24-well plates. The following day, cells were washed with phosphate-buffered saline (PBS). Cells were supplied with fresh medium every 2 days and incubated for 6 days. shAVPR1A-7 was used for Fig. 2 and fig. S3; shAVPR1A-3′UTR was used for fig. S4 (C and D). For assays of cell proliferation in response to AVP treatment, the indicated doses of AVP were added daily. For the AVPR1A overexpression assay, LNCaP (10,000 cells per well) were seeded in 24-well plates. The following day, cells were washed with PBS twice. Cells were cultured with 10% CSS. Medium was changed every 3 days, and cells were incubated for 15 days. Cells were trypsinized (Corning) and mixed with trypan blue (Gibco), and live cells were counted using a hemocytometer. Data represent at least three independent experiments performed in triplicate.

FLIPR calcium ion imaging assay

22Rv1, CWR-R1, PC3, DU145, and RWPE-1 cells were seeded in black-walled 384-well plates at a density of 10,000 cells per well in serum-free media. Twenty-four hours later, the Fluo-8 No Wash Calcium Assay Kit (ab112129, Abcam) was used according to the manufacturer's recommendations. The plate was then allowed to equilibrate to room temperature for 30 min before being analyzed with the FLIPR Tetra system. A 10-s reading of background fluorescence was performed before adding AVP or AVP and relcovaptan. After the addition, fluorescence intensity was recorded every second for at least 3 min. Final values represent the maximum recorded calcium response minus the minimum recorded calcium response for each well. Each experiment was performed in triplicate.

Plasmids and lentiviral production

The DNA constructs pLKO.1 shGFP, tet-pLKO.1 shGFP, shAR-V7, and shVAV3 were gifts from fellow scientists (see Acknowledgments). To generate the shRNA vector targeting *AVPR1A*, the sense and antisense oligonucleotides were synthesized (table S2). The oligonucleotides were annealed by heating to 95°C followed by slow cooling to room temperature. The annealed oligos were ligated into Age I– and Eco RI-digested pLKO.1 vector. For selection of stable cell line derivatives, cells were transduced with the appropriate constructs 24 hours after seeding. Forty-eight hours after transduction, cells were selected in puromycin (2.5 μg/ml) for a subsequent 48 to 72 hours. pCMV6-AVPR1A [full length complementary DNA (cDNA)] was obtained from TrueClone and subcloned into pQCXIN vector (Clontech) for retrovirus expression. Transduced cells were selected in G418 (1 mg/ml) for a subsequent 96 to 120 hours.

RNA isolation and RT-qPCR

Total RNA was harvested using the TRIzol method, according to the manufacturer's protocol (Invitrogen Life Technologies). Total RNA (1 μg) was reverse-transcribed using a High-Capacity cDNA Reverse Transcription kit (Thermo Fisher Scientific). Real-time PCR was performed using 100 ng of cDNA and ABI StepOnePlus. TaqMan probes from Thermo Fisher Scientific for *AVPR1A* (HS00176122) and *GAPDH* (HS99999905) were used. The comparative threshold cycle method was used to determine the relative expression of mRNA.

Immunoblotting

Cells or tumor samples were harvested in radioimmunoprecipitation assay buffer supplemented with β-mercaptoethanol. Samples were denatured at 95°C for 5 min. Samples for detecting HA-AVPR1A were not heated to prevent protein aggregation. Western blots were performed as previously described (7). Cleaved PARP (9541), phospho-ERK1/2 (4370), ERK1/2 (4696), phospho-CREB (9198), and CREB (9197) antibodies were purchased from Cell Signaling Technology. HSP90 was purchased from BD Transduction Laboratories (610419). HA (sc-805), cyclin A (sc-751), and actin (sc-1616) antibodies and hypoxanthine-guanine phosphoribosyltransferase-conjugated secondary antibodies were obtained from Santa Cruz Biotechnology.

Phosphoproteome kinase arrays

22Rv1 cells were plated at 3×10^6 in 150-mm plates (Corning) in medium containing 10% FBS. After 24-hour serum starvation, cells were pretreated with 1 μM relcovaptan or vehicle control, followed by treatment with 100 nM AVP or vehicle control. Samples of 200 μg of protein from each treatment group were subjected to Proteome Profiler Human Phospho-Kinase Arrays ARY003B (R&D Systems) following the manufacturer's protocol. Densitometry was performed using Adobe Photoshop Elements 14.

Subcutaneous and orthotopic xenograft experiments

Studies involving animals were conducted under a protocol approved by the Institutional Animal Care and Use Committee (IACUC) of the University of Miami and adhered to the National Institutes of Health (NIH) Guide for the Care and Use of Laboratory Animals. GFP/VAV3 VCaP xenografts were established as previously described (5). For LNCaP xenografts, 5- to 6-week-old nude mice (Envigo) were subcutaneously injected with 3×10^6 LNCaP cells expressing either empty vector ($n = 19$) or AVPR1A ($n = 19$) into both hind flanks with Matrigel (BD Biosciences). Tumors were measured three times per week by treatment-blinded staff. Mice were castrated when tumors measured 100 mm^3. Four weeks after castration, mice were euthanized and xenografts were collected for analysis. For the relcovaptan treatment study, 2×10^6 VCaP cells were injected with Matrigel subcutaneously into both hind flanks of intact SCID mice (Envigo). Mice were castrated when tumors measured 250 to 300 mm^3. Seven days after castration, mice were randomly assigned into vehicle ($n = 10$, 0.3% methylcellulose) or relcovaptan ($n = 13$, 50 mg/kg daily in 0.3% methylcellulose) groups. Tumors were measured three times per week by treatment-blinded staff. Mice were euthanized, and xenografts were collected after 14 days of treatment.

Circulating PSA was quantified from serum samples by an enzyme-linked immunosorbent assay (BC-1019, BioCheck Inc.). Immunofluorescent staining was performed using a Ki67 antibody (AB9260, Millipore) and mounted with 4′,6-diamidino-2-phenylindole (DAPI)–containing mounting medium (H-1500, VECTASHIELD). Samples were analyzed using ImageJ.

For orthotopic xenograft experiments, 10^6 luciferase-expressing C4-2B cells in PBS were injected into prostates of 5- to 6-week-old SCID mice (Envigo), and both testicles were removed during the surgery. Two weeks after surgery, mice were imaged by IVIS to confirm that C4-2B tumors were established and were subsequently randomly assigned to either the vehicle control group ($n = 9$) or the relcovaptan ($n = 10$) treatment group. Mice received either control vehicle or relcovaptan by daily oral gavage as described above. After 42 days of treatment, mice were euthanized and tumors were removed and imaged with IVIS.

Intratibial injection experiments

Studies involving animals were conducted under a protocol approved by the IACUC of Moffitt Cancer Center and adhered to the NIH Guide for the Care and Use of Laboratory Animals. Established methodology of intratibial injection was followed as previously described (42). Luciferase-expressing C4-2B cells (10^5 in 10 μl of saline) were inoculated into the tibias of castrated SCID mice. Contralateral limbs received sham injections of saline alone to serve as an internal baseline control for bone remodeling. One week after injection, bioluminescence was measured (IVIS200) to ensure equal tumor take, and subsequently the mice were randomized into vehicle control ($n = 7$; 0.3% methylcellulose in saline, daily oral gavage) and relcovaptan ($n = 8$, 50 mg/kg, daily oral gavage) groups. Bioluminescence was measured twice weekly as a readout for tumor growth. Individual mice were euthanized as their bioluminescence signal reached instrument detection limits [relative light units (RLU) = 2×10^7 ph^{-1} s^{-1} cm^{-2} sr^{-1}]. Remaining mice were euthanized after 83 days, and bone tissue was collected from all xenografted and sham-injected mice. High-resolution μCT were performed to analyze bone volume. Bone volumes were quantified by ImageJ. Tartrate-resistant acid phosphatase staining and pan-cytokeratin staining (C2562, Sigma-Aldrich) were performed to analyze bone remodeling and C4-2B tumor burden in the tibia.

Statistical analysis

All data were tested for normality. Two-tailed Student's *t* test was used to determine the significance of the difference between two groups of data. Student's *t* test of area under curve was used to determine significance of the difference between cell growth curves in Fig. 2A and fig. S3A. One-way ANOVA with Bonferroni correction was used to test the significance of differences among more than two groups of data. Log-rank test was used to test the significance of differences in mouse survival rates. Results are expressed as means ± SEM, and $P < 0.05$ was considered significant. Statistical analyses and graph plotting were carried out using Prism software version 6.01 (www.graphpad.com).

Supplementary Material

Refer to Web version on PubMed Central for supplementary material.

Acknowledgments:

We thank B. Wasserlauf and the Sylvester's Cancer Modeling Shared Resource of the University of Miami and S. Brothers and C.-H. Volmar and Sylvester's Molecular Therapeutics Shared Resource for advice and technical assistance. The services of the Pathology Research Resources Histology Laboratory were used. We thank G. Santiago and C. Coughlin for assistance with some experiments. We thank D. Kwon for statistical consulting. We thank E.M. Wilson (University of North Carolina, Chapel Hill, NC), K. Pienta (University of Michigan, Ann Arbor, MI), S. Plymate (University of Washington, Seattle, WA), and L. Chung (Cedar Sinai Medical Center, Los Angeles, CA) for the gifts of CWR-R1, VCaP, LNCaP-abl, and C4-2B cells, respectively. We thank P. Rai (University of Miami) for pLKO.1 shGFP and tet-pLKO.1 shGFP constructs, Y. Qiu (University of Maryland School of Medicine, Baltimore, MD) for shAR-V7 construct, and D. Billadeau (Mayo Clinic, Rochester, MN) for shVAV3 construct.

Funding: This work was supported by DOD W81XWH-14-1-0431 (to K.L.B.), VA Merit Review 1I01BX002773 (to K.L.B.), Sylvester Comprehensive Cancer Center Developmental Funds (to K.L.B.), Wallace H. Coulter Foundation (to K.L.B.), Florida Academic Cancer Center Alliance (to K.L.B., Y.D., and C.C.L.), Urology Care Foundation Research Scholar Award (to N.Z.), and predoctoral fellowships NIH F30AG038275F30 (to S.O.P.) and DOD W81XWH-11-1-0314 (to M.A.R.).

REFERENCES AND NOTES

1. Wang Q, Li W, Zhang Y, Yuan X, Xu K, Yu J, Chen Z, Beroukhim R, Wang H, Lupien M, Wu T, Regan MM, Meyer CA, Carroll JS, Manrai AK, Janne OA, Balk SP, Mehra R, Han B, Chinnaiyan AM, Rubin MA, True L, Fiorentino M, Fiore C, Loda M, Kantoff PW, Liu XS, Brown M, Androgen receptor regulates a distinct transcription program in androgen-independent prostate cancer. Cell 138, 245–256 (2009). [PubMed: 19632176]
2. Pomerantz MM, Li F, Takeda DY, Lenci R, Chonkar A, Chabot M, Cejas P, Vazquez F, Cook J, Shivdasani RA, Bowden M, Lis R, Hahn WC, Kantoff PW, Brown M, Loda M, Long HW, Freedman ML, The androgen receptor cistrome is extensively reprogrammed in human prostate tumorigenesis. Nat. Genet 47, 1346–1351 (2015). [PubMed: 26457646]
3. Lyons LS, Burnstein KL, Vav3, a Rho GTPase guanine nucleotide exchange factor, increases during progression to androgen independence in prostate cancer cells and potentiates androgen receptor transcriptional activity. Mol. Endocrinol 20, 1061–1072 (2006). [PubMed: 16384856]
4. Lyons LS, Rao S, Balkan W, Faysal J, Maiorino CA, Burnstein KL, Ligand-independent activation of androgen receptors by Rho GTPase signaling in prostate cancer. Mol. Endocrinol 22, 597–608 (2008). [PubMed: 18079321]
5. Rao S, Lyons LS, Fahrenholtz CD, Wu F, Farooq A, Balkan W, Burnstein KL, A novel nuclear role for the Vav3 nucleotide exchange factor in androgen receptor coactivation in prostate cancer. Oncogene 31, 716–727 (2012). [PubMed: 21765461]
6. Lin K-T, Gong J, Li CF, Jang T-H, Chen W-L, Chen H-J, Wang L-H, Vav3-rac1 signaling regulates prostate cancer metastasis with elevated Vav3 expression correlating with prostate cancer progression and posttreatment recurrence. Cancer Res. 72, 3000–3009 (2012). [PubMed: 22659453]
7. Peacock SO, Fahrenholtz CD, Burnstein KL, Vav3 enhances androgen receptor splice variant activity and is critical for castration-resistant prostate cancer growth and survival. Mol. Endocrinol 26, 1967–1979 (2012). [PubMed: 23023561]
8. Dehm SM, Tindall DJ, Alternatively spliced androgen receptor variants. Endocr. Relat. Cancer 18, R183–R196 (2011). [PubMed: 21778211]
9. Luo J, Attard G, Balk SP, Bevan C, Burnstein K, Cato L, Cherkasov A, De Bono JS, Dong Y, Gao AC, Gleave M, Heemers H, Kanayama M, Kittler R, Lang JM, Lee RJ, Logothetis CJ, Matusik R, Plymate S, Sawyers CL, Selth LA, Soule H, Tilley W, Weigel NL, Zoubeidi A, Dehm SM, Raj GV, Role of androgen receptor variants in prostate cancer: Report from the 2017 mission androgen receptor variants meeting. Eur. Urol 73, 715–723 (2018). [PubMed: 29258679]
10. Koshimizu T.-a., Nakamura K, Egashira N, Hiroyama M, Nonoguchi H, Tanoue A, Vasopressin V1a and V1b receptors: From molecules to physiological systems. Physiol. Rev 92, 1813–1864 (2012). [PubMed: 23073632]
11. North WG, Fay MJ, Du J, All three vasopressin receptor sub-types are expressed by small-cell carcinoma. Adv. Exp. Med. Biol 449, 335–338 (1998). [PubMed: 10026822]

12. Keegan BP, Akerman BL, Pequeux C, North WG, Provasopressin expression by breast cancer cells: Implications for growth and novel treatment strategies. Breast Cancer Res. Treat 95, 265–277 (2006). [PubMed: 16331351]
13. Fay MJ, Friedmann AS, Yu XM, North WG, Vasopressin and vasopressin-receptor immunoreactivity in small-cell lung carcinoma (SCCL) cell lines: Disruption in the activation cascade of V1a-receptors in variant SCCL. Cancer Lett. 82, 167–174 (1994). [PubMed: 8050087]
14. Birnbaumer M, Vasopressin receptors. Trends Endocrinol. Metab 11, 406–410 (2000). [PubMed: 11091117]
15. Thibonnier M, Auzan C, Madhun Z, Wilkins P, Berti-Mattera L, Clauser E, Molecular cloning, sequencing, and functional expression of a cDNA encoding the human V1a vasopressin receptor. J. Biol. Chem 269, 3304–3310 (1994). [PubMed: 8106369]
16. Thibonnier M, Conarty DM, Plesnicher CL, Mediators of the mitogenic action of human V(1) vascular vasopressin receptors. Am. J. Physiol. Heart Circ. Physiol 279, H2529–H2539 (2000). [PubMed: 11045991]
17. North WG, Fay MJ, Longo K, Du J, Functional vasopressin V1 type receptors are present in variant as well as classical forms of small-cell carcinoma. Peptides 18, 985–993 (1997). [PubMed: 9357056]
18. North WG, Fay MJ, Du J, MCF-7 breast cancer cells express normal forms of all vasopressin receptors plus an abnormal V_2R. Peptides 20, 837–842 (1999). [PubMed: 10477084]
19. Decaux G, Soupart A, Vassart G, Non-peptide arginine-vasopressin antagonists: the vaptans. Lancet 371, 1624–1632 (2008). [PubMed: 18468546]
20. Hayoz D, Bizzini G, Noël B, Depairon M, Burnier M, Fauveau C, Rouillon A, Brouard R, Brunner HR, Effect of SR 49059, a V1a vasopressin receptor antagonist, in Raynaud's phenomenon. Rheumatology 39, 1132–1138 (2000). [PubMed: 11035135]
21. Brouard R, Laporte V, Serradeil Le Gal C, Pignol R, Jang H, Donat F, Lockwood G, Fournie D, Dreux F, Safety, tolerability, and pharmacokinetics of SR 49059, a V1a vasopressin receptor antagonist, after repeated oral administration in healthy volunteers. Adv. Exp. Med. Biol 449, 455–465 (1998). [PubMed: 10026839]
22. Brouard R, Bossmar T, Fournie-Lloret D, Chassard D, Åkerlund M, Effect of SR49059, an orally active V_{1a} vasopressin receptor antagonist, in the prevention of dysmenorrhoea. BJOG 107, 614–619 (2000). [PubMed: 10826575]
23. Beltran H, Prandi D, Mosquera JM, Benelli M, Puca L, Cyrta J, Marotz C, Giannopoulou E, Chakravarthi BVSK, Varambally S, Tomlins SA, Nanus DM, Tagawa ST, Van Allen EM, Elemento O, Sboner A, Garraway LA, Rubin MA, Demichelis F, Divergent clonal evolution of castration-resistant neuroendocrine prostate cancer. Nat. Med 22, 298–305 (2016). [PubMed: 26855148]
24. Tamura K, Furihata M, Tsunoda T, Ashida S, Takata R, Obara W, Yoshioka H, Daigo Y, Nasu Y, Kumon H, Konaka H, Namiki M, Tozawa K, Kohri K, Tanji N, Yokoyama M, Shimazui T, Akaza H, Mizutani Y, Miki T, Fujioka T, Shuin T, Nakamura Y, Nakagawa H, Molecular features of hormone-refractory prostate cancer cells by genome-wide gene expression profiles. Cancer Res. 67, 5117–5125 (2007). [PubMed: 17545589]
25. Chandran UR, Ma C, Dhir R, Bisceglia M, Lyons-Weiler M, Liang W, Michalopoulos G, Becich M, Monzon FA, Gene expression profiles of prostate cancer reveal involvement of multiple molecular pathways in the metastatic process. BMC Cancer 7, 64 (2007). [PubMed: 17430594]
26. Fahrenholtz CD, Beltran PJ, Burnstein KL, Targeting IGF-IR with ganitumab inhibits tumorigenesis and increases durability of response to androgen-deprivation therapy in VCaP prostate cancer xenografts. Mol. Cancer Ther 12, 394–404 (2013). [PubMed: 23348048]
27. Loberg RD, St John LN, Day LL, Neeley CK, Pienta KJ, Development of the VCaP androgen-independent model of prostate cancer. Urol. Oncol 24, 161–168 (2006). [PubMed: 16520280]
28. Watson PA, Chen YF, Balbas MD, Wongvipat J, Socci ND, Viale A, Kim K, Sawyers CL, Constitutively active androgen receptor splice variants expressed in castration-resistant prostate cancer require full-length androgen receptor. Proc. Natl. Acad. Sci. U.S.A 107, 16759–16765 (2010). [PubMed: 20823238]

29. Cerami E, Gao J, Dogrusoz U, Gross BE, Sumer SO, Aksoy BA, Jacobsen A, Byrne CJ, Heuer ML, Larsson E, Antipin Y, Reva B, Goldberg AP, Sander C, Schultz N, The cBio cancer genomics portal: An open platform for exploring multidimensional cancer genomics data. Cancer Discov. 2, 401–404 (2012). [PubMed: 22588877]
30. Gao J, Aksoy BA, Dogrusoz U, Dresdner G, Gross B, Sumer SO, Sun Y, Jacobsen A, Sinha R, Larsson E, Cerami E, Sander C, Schultz N, Integrative analysis of complex cancer genomics and clinical profiles using the cBioPortal. Sci. Signal 6, pl1 (2013). [PubMed: 23550210]
31. Cancer Genome Atlas Research Network, The Molecular Taxonomy of Primary Prostate Cancer. Cell 163, 1011–1025 (2015). [PubMed: 26544944]
32. Antonarakis ES, Lu C, Wang H, Luber B, Nakazawa M, Roeser JC, Chen Y, Mohammad TA, Chen Y, Fedor HL, Lotan TL, Zheng Q, De Marzo AM, Isaacs JT, Isaacs WB, Nadal R, Paller CJ, Denmeade SR, Carducci MA, Eisenberger MA, Luo J, AR-V7 and resistance to enzalutamide and abiraterone in prostate cancer. N. Engl. J. Med 371, 1028–1038 (2014). [PubMed: 25184630]
33. Racila E, Euhus D, Weiss AJ, Rao C, McConnell J, Terstappen LWMM, Uhr JW, Detection and characterization of carcinoma cells in the blood. Proc. Natl. Acad. Sci. U.S.A 95, 4589–4594 (1998). [PubMed: 9539782]
34. Horoszewicz JS, Leong SS, Kawinski E, Karr JP, Rosenthal H, Chu TM, Mirand EA, Murphy GP, LNCaP model of human prostatic carcinoma. Cancer Res. 43, 1809–1818 (1983). [PubMed: 6831420]
35. Serradeil-Le Gal C, Wagnon J, Garcia C, Lacour C, Guiraudou P, Christophe B, Villanova G, Nisato D, Maffrand JP, Le Fur G, Biochemical and pharmacological properties of SR 49059, a new, potent, nonpeptide antagonist of rat and human vasopressin V1a receptors. J. Clin. Invest 92, 224–231 (1993). [PubMed: 8392086]
36. Hiroyama M, Wang S, Aoyagi T, Oikawa R, Sanbe A, Takeo S, Tanoue A, Vasopressin promotes cardiomyocyte hypertrophy via the vasopressin V_{1A} receptor in neonatal mice. Eur. J. Pharmacol 559, 89–97 (2007). [PubMed: 17275806]
37. Chen Y, Xu F, Zhang L, Wang X, Wang Y, Woo AY-H, Zhu W, GRK2/β-arrestin mediates arginine vasopressin-induced cardiac fibroblast proliferation. Clin. Exp. Pharmacol. Physiol 44, 285–293 (2017). [PubMed: 27862165]
38. Li X, Chan TO, Myers V, Chowdhury I, Zhang X-Q, Song J, Zhang J, Andrel J, Funakoshi H, Robbins J, Koch WJ, Hyslop T, Cheung JY, Feldman AM, Controlled and cardiac-restricted overexpression of the arginine vasopressin V1A receptor causes reversible left ventricular dysfunction through $G\alpha_q$-mediated cell signaling. Circulation 124, 572–581 (2011). [PubMed: 21747049]
39. Zhang L, Wang X, Cao H, Chen Y, Chen X, Zhao X, Xu F, Wang Y, Woo A-Y, Zhu W, Vasopressin V_{1A} receptor mediates cell proliferation through GRK2-EGFR-$ERK_{1/2}$ pathway in A7r5 cells. Eur. J. Pharmacol 792, 15–25 (2016). [PubMed: 27773680]
40. Rucci N, Angelucci A, Prostate cancer and bone: The elective affinities. Biomed. Res. Int 2014, 167035 (2014). [PubMed: 24971315]
41. Tamma R, Sun L, Cuscito C, Lu P, Corcelli M, Li J, Colaianni G, Moonga SS, Di Benedetto A, Grano M, Colucci S, Yuen T, New MI, Zallone A, Zaidi M, Regulation of bone remodeling by vasopressin explains the bone loss in hyponatremia. Proc. Natl. Acad. Sci. U.S.A 110, 18644–18649 (2013). [PubMed: 24167258]
42. Thiolloy S, Edwards JR, Fingleton B, Rifkin DB, Matrisian LM, Lynch CC, An osteoblast-derived proteinase controls tumor cell survival via TGF-beta activation in the bone microenvironment. PLOS ONE 7, e29862 (2012). [PubMed: 22238668]
43. Greenberg A, Verbalis JG, Vasopressin receptor antagonists. Kidney Int. 69, 2124–2130 (2006). [PubMed: 16672911]
44. Thibonnier M, Plesnicher CL, Berrada K, Berti-Mattera L, Role of the human V_1 vasopressin receptor COOH terminus in internalization and mitogenic signal transduction. Am. J. Physiol. Endocrinol. Metab 281, E81–E92 (2001). [PubMed: 11404225]
45. Kumar AP, Bhaskaran S, Ganapathy M, Crosby K, Davis MD, Kochunov P, Schoolfield J, Yeh I-T, Troyer DA, Ghosh R, Akt/cAMP-responsive element binding protein/cyclin D1 network: A novel target for prostate cancer inhibition in transgenic adenocarcinoma of mouse prostate model

mediated by Nexrutine, a *Phellodendron amurense* bark extract. Clin. Cancer Res 13, 2784–2794 (2007). [PubMed: 17473212]

46. James MA, Lu Y, Liu Y, Vikis HG, You M, RGS17, an overexpressed gene in human lung and prostate cancer, induces tumor cell proliferation through the cyclic AMP-PKA-CREB pathway. Cancer Res. 69, 2108–2116 (2009). [PubMed: 19244110]
47. Deng X, Liu H, Huang J, Cheng L, Keller ET, Parsons SJ, Hu C-D, Ionizing radiation induces prostate cancer neuroendocrine differentiation through interplay of CREB and ATF2: implications for disease progression. Cancer Res. 68, 9663–9670 (2008). [PubMed: 19047143]
48. Park M-H, Lee H-S, Lee C-S, You ST, Kim D-J, Park B-H, Kang MJ, Heo WD, Shin E-Y, Schwartz MA, Kim E-G, p21-Activated kinase 4 promotes prostate cancer progression through CREB. Oncogene 32, 2475–2482 (2013). [PubMed: 22710715]
49. Sang M, Hulsurkar M, Zhang X, Song H, Zheng D, Zhang Y, Li M, Xu J, Zhang S, Ittmann M, Li W, GRK3 is a direct target of CREB activation and regulates neuroendocrine differentiation of prostate cancer cells. Oncotarget 7, 45171–45185 (2016). [PubMed: 27191986]
50. Huang W-C, Wu D, Xie Z, Zhau HE, Nomura T, Zayzafoon M, Pohl J, Hsieh C-L, Weitzmann MN, Farach-Carson MC, Chung LWK, β2-microglobulin is a signaling and growth-promoting factor for human prostate cancer bone metastasis. Cancer Res. 66, 9108–9116 (2006). [PubMed: 16982753]
51. Wu D, Zhau HE, Huang W-C, Iqbal S, Habib FK, Sartor O, Cvitanovic L, Marshall FF, Xu Z, Chung LW, cAMP-responsive element-binding protein regulates vascular endothelial growth factor expression: implication in human prostate cancer bone metastasis. Oncogene 26, 5070–5077 (2007). [PubMed: 17310988]
52. Desdouets C, Matesic G, Molina CA, Foulkes NS, Sassone-Corsi P, Brechot C, Sobczak-Thepot J, Cell cycle regulation of cyclin A gene expression by the cyclic AMP-responsive transcription factors CREB and CREM. Mol. Cell. Biol 15, 3301–3309 (1995). [PubMed: 7760825]
53. Kibler KV, Jeang K-T, CREB/ATF-dependent repression of cyclin a by human T-cell leukemia virus type 1 Tax protein. J. Virol 75, 2161–2173 (2001). [PubMed: 11160720]
54. Nagata D, Suzuki E, Nishimatsu H, Satonaka H, Goto A, Omata M, Hirata Y, Transcriptional activation of the *cyclin D1* gene is mediated by multiple *cis*-elements, including SP1 sites and a cAMP-responsive element in vascular endothelial cells. J. Biol. Chem 276, 662–669 (2001). [PubMed: 11024050]
55. Serradeil-Le Gal C, Raufaste D, Marty E, Garcia C, Maffrand JP, Le Fur G, Binding of (^{3}H) SR 49059, a potent nonpeptide vasopressin V_{1a} antagonist, to rat and human liver membranes. Biochem. Biophys. Res. Commun 199, 353–360 (1994). [PubMed: 8123034]
56. Engin E, Treit D, Dissociation of the anxiolytic-like effects of Avpr1a and Avpr1b receptor antagonists in the dorsal and ventral hippocampus. Neuropeptides 42, 411–421 (2008). [PubMed: 18508119]
57. Hawtin SR, Davies ARL, Matthews G, Wheatley M, Identification of the glycosylation sites utilized on the V-1a vasopressin receptor and assessment of their role in receptor signalling and expression. Biochem. J 357, 73–81 (2001). [PubMed: 11415438]

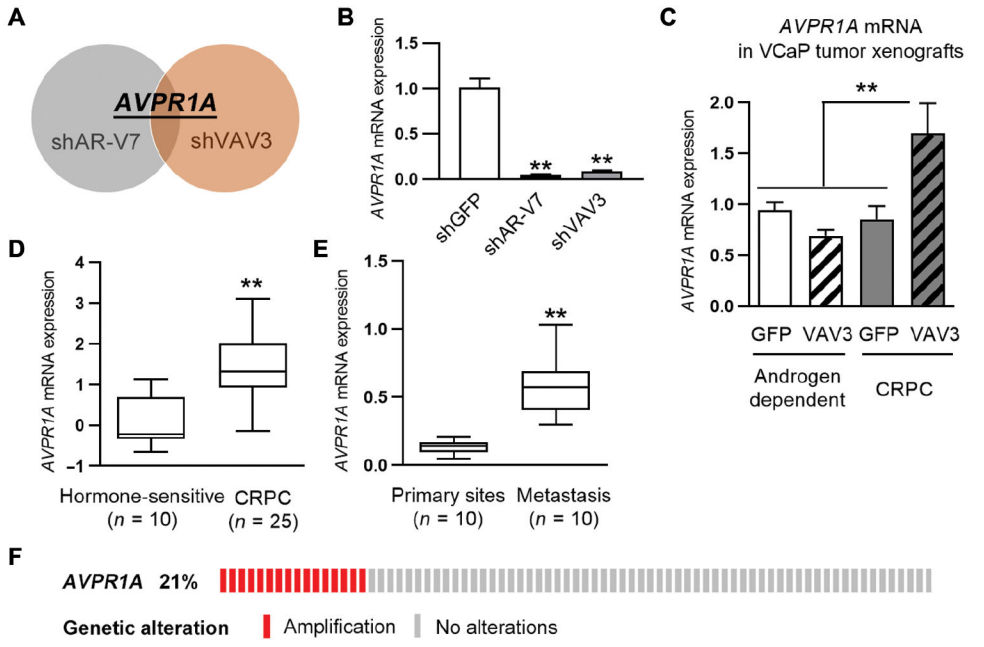

Fig. 1. *AVPR1A* is regulated by the AR coactivator VAV3 and AR-V7 and is increased in advanced human PC.

(**A**) Gene expression profiling revealed that doxycycline-induced depletion of AR-V7 or VAV3 in 22Rv1 cells resulted in decreased *AVPR1A* mRNA (Student's *t* test, $P < 0.05$). (**B**) VAV3 or AR-V7 was stably depleted by shRNA in 22Rv1 cells analyzed by reverse transcriptase quantitative polymerase chain reaction (RT-qPCR) for *AVPR1A* mRNA (Student's *t* test, $^{**}P < 0.01$). One experiment was done in triplicate. (**C**) *AVPR1A* mRNA was quantified in VCaP xenograft tumors with (VAV3) or without (GFP) VAV3 overexpression harvested before castration (androgen dependent) or at the end of the study (CRPC). The following xenograft tissues were evaluated: androgen-dependent/GFP ($n = 3$), androgen-dependent/VAV3 ($n = 3$), CRPC/GFP ($n = 5$), and CRPC/VAV3 ($n = 7$) [one-way analysis of variance (ANOVA) with Bonferroni correction, $^{**}P < 0.01$]. (**D**) Tamura PC datasets were obtained and analyzed using National Center for Biotechnology Information (NCBI) Gene Expression Omnibus (GEO) (24) to show *AVPR1A* mRNA in human hormone-sensitive specimens versus CRPC samples ($^{**}P < 0.01$). (**E**) Chandran PC datasets were obtained and analyzed using NCBI GEO (25) to show *AVPR1A* mRNA in human primary site (prostate) specimens versus metastatic samples ($^{**}P < 0.01$). (**F**) *AVPR1A* gene is amplified in 21% of metastatic CRPC tumors in the Beltran *et al.* (23) human CRPC dataset (81 patients with metastatic CRPC). Data were retrieved and analyzed using the cBioPortal ($^{**}P < 0.01$) (29, 30).

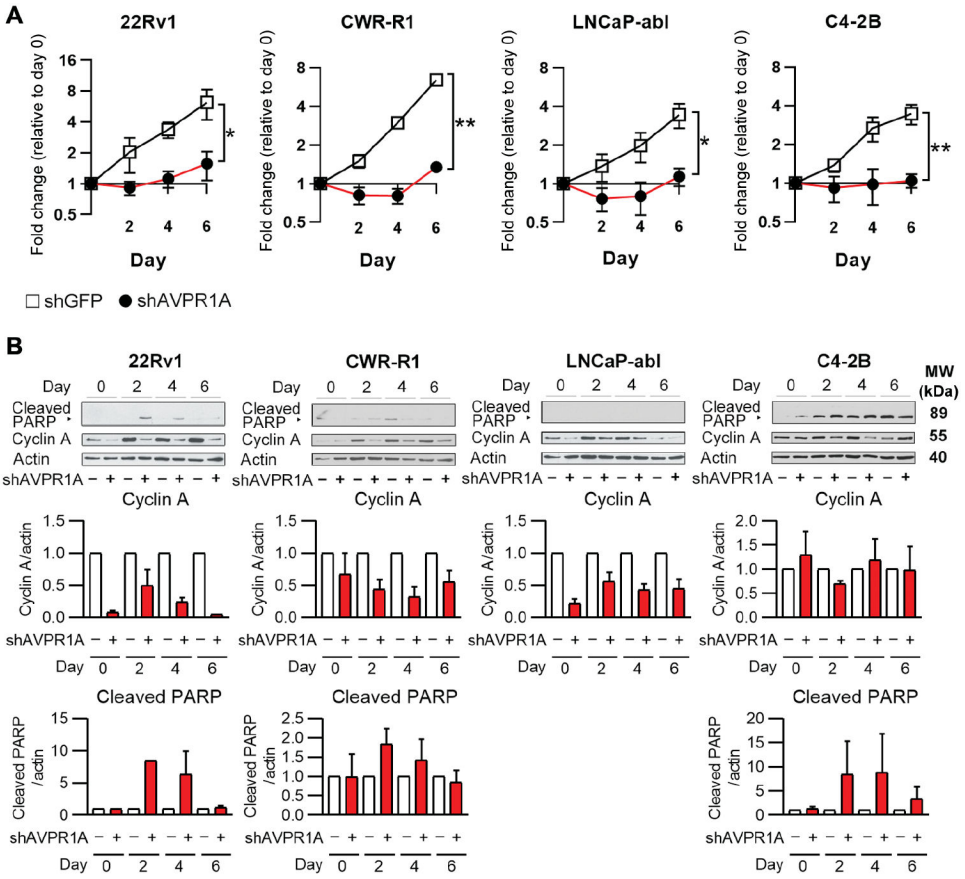

Fig. 2. Depletion of AVPR1A decreases CRPC cell proliferation.

(**A**) AR-positive CRPC cell lines were transduced with shAVPR1A or shGFP (negative control), followed by cell counting on the indicated days. Cell numbers were normalized to day 0 for each time point. □, shGFP; •, shAVPR1A. Summary of three independent experiments performed in triplicate is shown (Student's *t* test, $*P < 0.05$ and $**P < 0.01$). (**B**) Cell cycle marker cyclin A and apoptosis marker cleaved PARP were analyzed by immunoblotting. Representative blots of at least three independent experiments are shown. Cyclin A and cleaved PARP expression from blots were quantified and normalized to actin as the sample loading control. Graphs are summaries of at least three independent experiments. In cases where protein expression was undetectable, only $n = 2$ data points were able to be quantified. All the quantification data are included in the data file S1. MW, molecular weight.

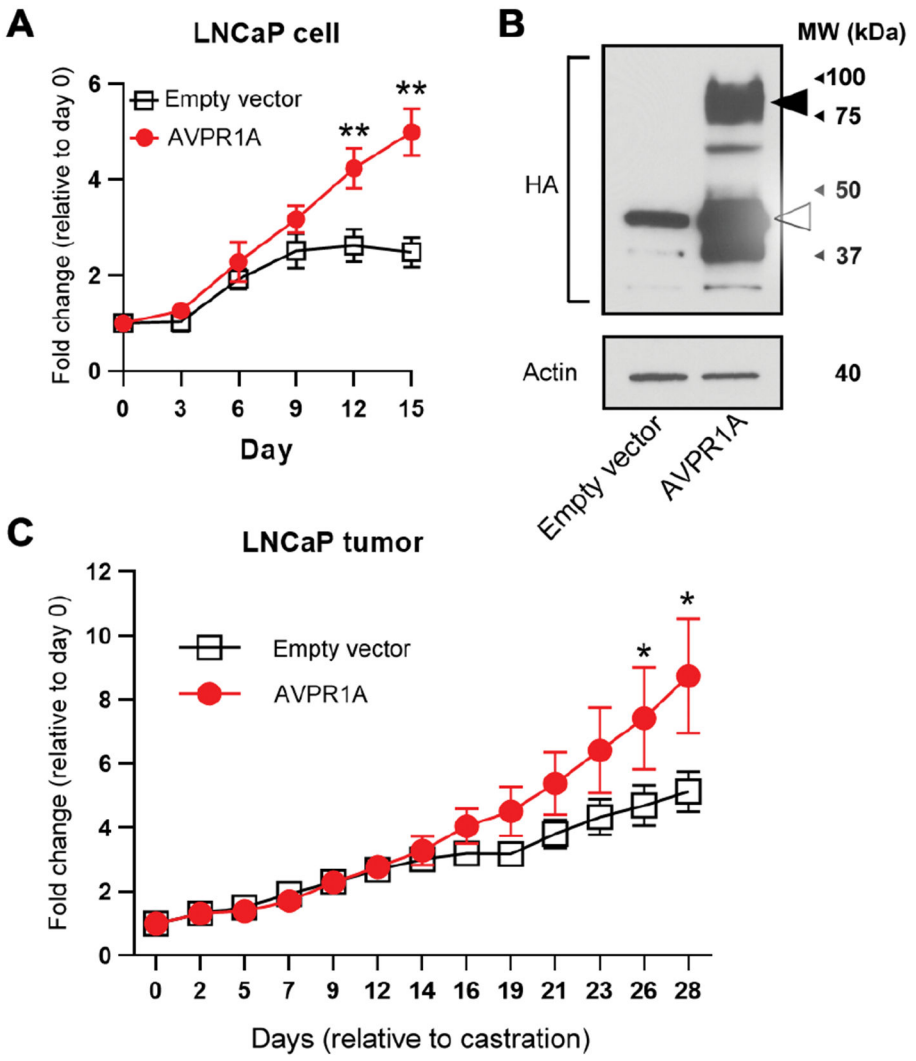

Fig. 3. AVPR1A confers castration resistance in vitro and in vivo.

(**A**) Androgen-dependent LNCaP cells stably expressing either empty vector or AVPR1A were cultured in medium depleted of androgen (CSS). Cells were counted on the indicated days. Summary of four independent experiments each performed in triplicate is shown (Student's *t* test, $^{**}P < 0.01$). (**B**) Expression of HA-tagged AVPR1A was analyzed by immunoblotting with HA antibody. AVPR1A is 418 amino acids in size and is glycosylated (57). Open arrowhead indicates unmodified AVPR1A (418 amino acids), and the black arrowhead indicates glycosylated AVPR1A. (**C**) LNCaP/AVPR1A or LNCaP/empty vector cells were injected subcutaneously into immunocompromised mice. Mice were castrated when tumors reached 100 mm^3. LNCaP xenograft tumor volumes (empty vector, $n = 19$; AVPR1A, $n = 19$) were measured at the indicated time points (up to 4 weeks) after castration, and fold change was plotted (compared to tumor volume at the time of castration on day 0). Tumor growth of the empty vector group was compared to that of the AVPR1A group at the same time points (Student's *t* test, $^{*}P < 0.05$).

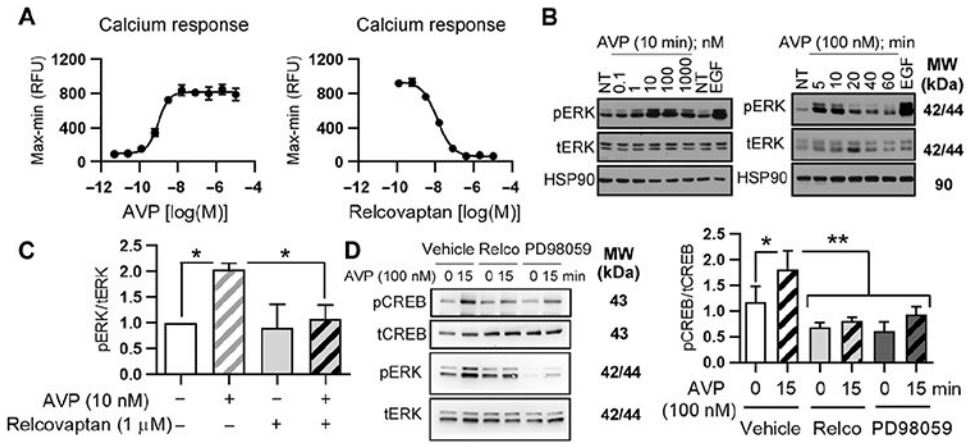

Fig. 4. AVPR1A antagonist, relcovaptan, blocks AVP-mediated calcium flux and ERK/CREB activation in CRPC cells.

(**A**) 22Rv1 cells were cultured in serum-free medium for 24 hours, followed by treatment with AVP at indicated concentrations or 4.5 nM AVP and relcovaptan at indicated concentrations before measurement of calcium fluorescence. Data are presented in relative fluorescence units (RFUs). Graphs shown are representative of three independent experiments performed in triplicate. (**B**) 22Rv1 cells serum-starved for 48 hours were treated with the indicated concentrations of AVP or no (vehicle) treatment (NT) or were treated with 100 nM AVP for indicated time periods. Epidermal growth factor (EGF; 10 ng/ml) served as a positive control. Blots shown are representative of two independent experiments. (**C**) 22Rv1 cells serum-starved for 24 hours were pretreated with 1 μM relcovaptan or vehicle (−) for 30 min, followed by 25-min treatment with 10 nM AVP or vehicle (−). Quantification of phospho-extracellular signal–regulated kinase 1/2 (ERK1/2) was summarized from three independent experiments (one-way ANOVA with Bonferroni correction, $*P < 0.05$). (**D**) 22Rv1 cells serum-starved for 24 hours were pretreated for 30 min with 10 μM relcovaptan, 10 μM PD98059, or vehicle, followed by 15-min treatment with 100 nM AVP or vehicle (−). Quantification of phospho–cyclic adenosine monophosphate response element–binding protein (CREB) was summarized from four independent experiments (one-way ANOVA with Bonferroni correction, $*P < 0.05$ and $**P < 0.01$).

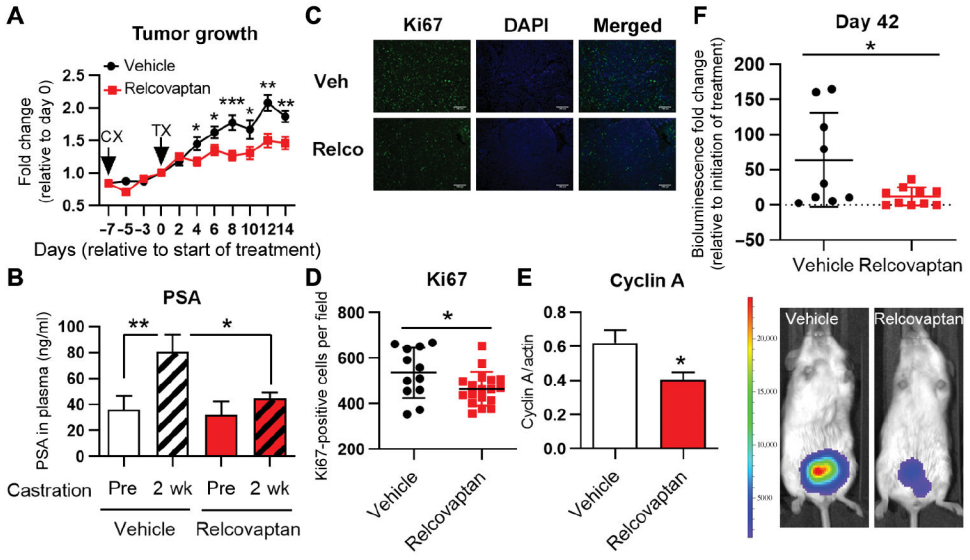

Fig. 5. Relcovaptan inhibits early emergent and established CRPC growth in vivo.

(**A**) Subcutaneous VCaP xenografts (bilateral) were established in SCID mice, and mice were castrated (CX) when tumors reached 250 to 300 mm^3. Vehicle or relcovaptan treatment (TX) was initiated 7 days after castration and continued for 14 days. Fold changes (relative to day 0) in tumor volume of vehicle- ($n = 10$) and relcovaptan-treated ($n = 13$) mice were calculated and plotted. Tumors from vehicle- and relcovaptan-treated mice were compared at the same time points. (Student's *t* test, $*P < 0.05$, $**P < 0.01$, and $***P < 0.001$). (**B**) Circulating PSA was measured in mice at the time of castration (pre) and at the time of sacrifice (2 weeks) (one-way ANOVA with Bonferroni correction, $*P < 0.05$ and $**P < 0.01$). (**C**) Tumor samples were subjected to immunofluorescent staining of Ki67 (green) and 4′,6-diamidino-2-phenylindole (DAPI) (blue). Scale bars, 100 μm. (**D**) Ki67-positive cell numbers in each field were quantified (Student's *t* test, $*P < 0.05$). (**E**) Cyclin A protein expression in tumors from vehicle- and relcovaptan-treated mice was analyzed by immunoblotting and quantified (Student's *t* test, $*P < 0.05$). Graph is a summary of the quantified data of all the tumor samples (11 tumors from vehicle-treated mice and 17 tumors from relcovaptan-treated mice). (**F**) C4-2B cells were inoculated into mouse prostates, and mice were castrated. Two weeks later, after tumors were established as defined by in vivo imaging system (IVIS) signal, mice were randomized and treated with vehicle or relcovaptan for 42 days. Mice were euthanized, and tumors were dissected out and imaged ex vivo using IVIS. Tumor growth of vehicle- ($n = 9$) and relcovaptan-treated ($n = 10$) animals was calculated as the bioluminescence at the end of the study compared to the initiation of treatment (top) (Student's *t* test, $*P < 0.05$). Representative IVIS images at day 42 are shown (bottom).

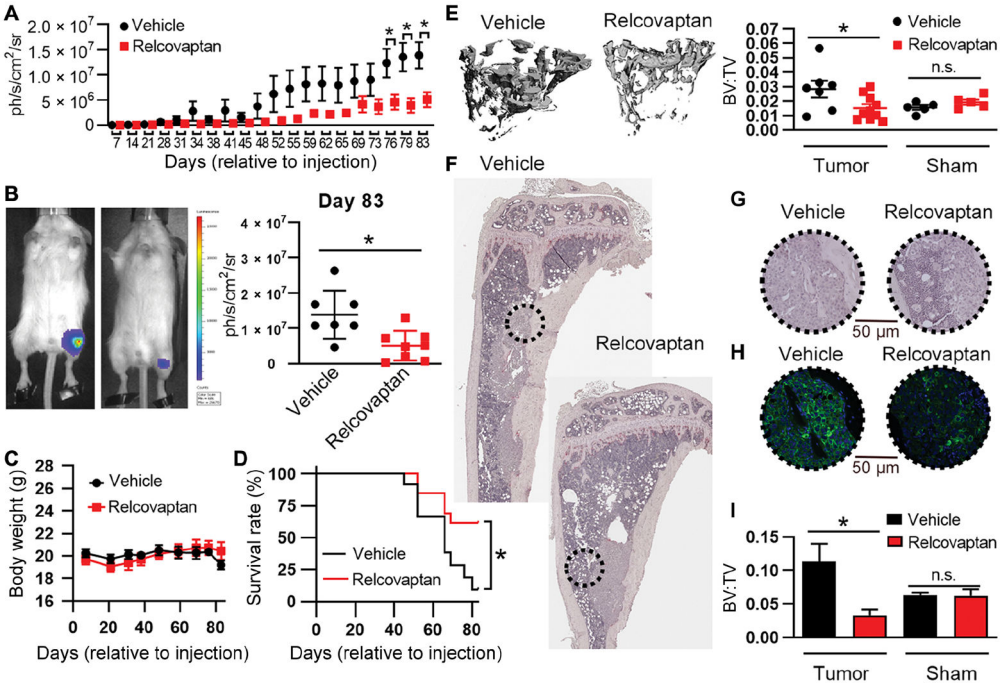

Fig. 6. Relcovaptan decreases the growth of bone CRPC and protects against bone CRPC-induced osteogenesis.

(**A**) SCID mice were castrated and, 1 week later, intratibially inoculated with luciferase-expressing C4-2B CRPC cells. Mice were randomized into vehicle ($n = 7$) and relcovaptan groups ($n = 8$) and treated daily for 83 days. Luminescence was measured twice weekly over the course of the study and compared between mice treated with relcovaptan and vehicle at each time point (Student's t test, $^*P < 0.05$). (**B**) Representative images (left) and luminescence quantitation (right) from vehicle- and relcovaptan-treated groups at day 83 are shown (Student's t test, $^*P < 0.05$). (**C**) Body weights were measured on a weekly basis. (**D**) Survival curves are shown for all mice treated with relcovaptan or vehicle (log-rank test, $^*P < 0.05$). (**E**) μCT scan analysis was performed on tibias from vehicle- and relcovaptan-treated mice bearing C4-2B bone metastases and contralateral tibias that received sham injections of saline (Student's t test, $^*P < 0.05$; n.s., not significant). (**F** to **H**) Gross micrograph illustrates tumor burden by tartrate-resistant acid phosphatase staining in each group (F), dashed circle represents area of magnification (G), and pan-cytokeratin (green) indicates C4-2B cells (H). (**I**) Ratio of trabecular bone volume (BV) to total volume (TV) in sections derived from the vehicle- and relcovaptan-treated groups was quantified (Student's t test, $^*P < 0.05$).